COMMUNICATIONS IN SCIENCE AND TECHNOLOGY
Homepage: cst.kipmi.or.id

The effect of pH on anthocyanin extraction from *Clitoria ternatea L.* and polyetherimide polymer membrane electrolyte on the efficiency of dye-sensitized solar cells (DSSCs)

Nita Kusumawati[a,*], Pirim Setiarso[a], Samik Samik[a], Muhamad Syariffuddien Zuhrie[b], AR. Sella Auliya[c], Khofifatul Rahmawati[a], Achmad Naufal Al Hafidl[a], Muchamad Sabilah Hanafi[a]

[a]*Department of Chemistry, Universitas Negeri Surabaya, Surabaya 60231, Indonesia*
[b]*Department of Electrical Engineering, Universitas Negeri Surabaya, Surabaya 60231, Indonesia*
[c]*Department of Mathematics, Universitas Islam Darul `Ulum Lamongan, Lamongan 71062, Indonesia*

Article history:
Received: 13 January 2026 / Received in revised form: 27 April 2026 / Accepted: 27 April 2026

Abstract

This present study investigates the effect of pH variation (2-12) on anthocyanin extraction from *Clitoria ternatea L.* and polyetherimide (PEI) polymer membrane electrolyte performance in dye-sensitized solar cells (DSSCs). The extraction of anthocyanin was conducted through the utilization of microwave-assisted extraction (MAE) at 280 watts for 15 minutes, employing a distilled water ratio of 1:20 ratio. This was followed by a systematic pH conditioning procedure. The characterization employed a range of analytical techniques, including UV-Vis spectrophotometry (400-800 nm), FTIR (4000-500 cm^{-1}), cyclic voltammetry for HOMO-LUMO analysis, SEM (1,000×-10,000× magnification), XRD for crystallinity determination, DSC for thermal stability (60-450°C), and electrochemical impedance spectroscopy. Results obtained demonstrated that pH 4 anthocyanin exhibited maximum dual absorption peaks at 571.21 nm and 612.85 nm, representing the magenta-colored quinoidal base structure with superior light-harvesting capabilities. The FTIR analysis confirmed the presence of stable functional groups, including O-H stretching (3338.08 cm^{-1}), C=O stretching (1710 cm^{-1}), and aromatic C=C (1416.91 cm^{-1}) across all pH conditions without new chemical bond formation. The pH 4 dye demonstrated the narrowest energy bandgap (0.1316 eV) with HOMO at -4.1597 eV and LUMO at -4.0281 eV, optimally aligned with the TiO_2 conduction band (-4.0 eV) for efficient electron injection. The PEI membrane exhibited asymmetric morphology with 12.77% crystallinity, a hierarchical porous structure, and excellent thermal stability up to 500°C. The performance of the DSCC reached its maximum at a pH of 4, with efficiency η = 2.37%, Voc = 597 mV, Jsc = 0.0119 mA/cm^2, FF = 5.60%, and minimum charge transfer resistance Rct = 100–150 Ω. These findings demonstrate that pH 4 optimization is critical for enhancing the efficiency of DSSC through quinoidal base formation, enhanced molecular conjugation, and accelerated charge transfer processes in environmentally sustainable photovoltaic systems.

Keywords: Clitoria ternatea L.; anthocyanin quinoidal base; polyetherimide membrane; pH-dependent photosensitization; DSSC efficiency optimization

1. Introduction

The escalating challenges of climate change and the necessity for energy security have driven the search for alternative energy sources. It is projected that global energy demand will increase by 50% by 2050, with 80% of global energy needs still reliant on fossil fuels [1]. This has led to a surge in interest in renewable energy sources, particularly solar cells. Dye-sensitized solar cells (DSSCs) have emerged as a promising technology due to their light absorption capability, low cost, and simple manufacturing process [2].

Conversion of solar energy into electricity by DSSCs utilizing photosensitive dyes involves several key components including a glass substrate, transparent conductor, TiO_2 nanoparticles, electrolyte, counter electrode, and natural dye. This present study employs a PEI-based membrane electrolyte due to its significant stability advantages, as highlighted by Kusumawati et al. (2019) [3]. PEI membranes demonstrate elevated chemical and thermal stability (up to 500°C), excellent ionic conductivity, and a porous structure that prevents electrolyte leakage while facilitating electron transfer [4]. Their low crystallinity (12.77%) further supports electrolyte retention and high conductivity, making PEI effective in addressing solvent evaporation and leakage issues for long-term DSSC performance [5].

It is evident that anthocyanin-based natural dyes, which are derived from plants serve as an eco-friendly and cost-effective alternative to synthetic dyes [6]. These pigments, found in brightly colored fruits and flowers, exhibit strong light

* Corresponding author.
Email: nitakusumawati@unesa.ac.id
https://doi.org/10.21924/cst.11.1.2026.1890

absorption, particularly cyanidins and their derivatives, with the added benefits of wide availability, low cost, and minimal environmental impact.

When exposed to light exposure, dye molecules that are anchored to the TiO_2 excite electrons from the HOMO to the LUMO, thereby injecting them into the conduction band of TiO_2. The electrons flow through TiO_2 towards the conductive substrate and counter electrode, generating electric current. The electrolyte regenerates oxidized dye and accepts electrons from the counter electrode through a platinum-catalyzed reduction process [7,8].

Research on natural dye-based DSSCs has been rapidly advancing. Kusumawati et al. (2020) investigated the effect of polyetherimide membrane composition on DSSC efficiency using anthocyanin extract from butterfly pea (*Clitoria ternatea L.*), achieving a maximum energy conversion efficiency of 1.66% [4]. In a subsequent study, Kusumawati et al. (2023) utilized butterfly pea anthocyanin extract at a 1:6 ratio (flower:solvent), yielding an enhanced efficiency of 1.69% [9]. Kumar et al. (2024) examined the impact of extraction solvents and soaking duration on the performance of anthocyanin dye. This study reported efficiencies of 0.87% and 0.92% for DSSCs utilizing dyes from *Kigelia africana* and *Hibiscus sabdariffa*, respectively, which were extracted with citric acid [10]. Rahmawati et al. (2025) reported that a ternary combination of natural dyes extracted from *Caesalpinia sappan L., Dracaena angustifolia*, and *Clitoria ternatea L.* achieved the highest efficiency of 3.24% [8].

Despite the fact that previous studies have examined anthocyanin performance in dye-based solar cells, the effect of pH on electron density across diverse anthocyanin molecular forms in DSSCs remains unexplored. In this study, the pH of the anthocyanin solution was varied to evaluate its influence on photovoltaic performance, characterized utilizing UV-Vis spectrophotometry, FTIR, cyclic voltammetry, SEM, XRD, DSC, and EIS. This understanding is expected to contribute to the design of novel materials for dyes, electrolytes, anodes, and cathodes in DSSC applications.

2. Materials and Methods

2.1. Materials

The materials employed in this study include polyetherimide (PEI) (molecular weight 354,000) (≥99% purity; Merck, Germany), N-polyetherimide (Germany), and methyl-2-pyrrolidone (NMP) (≥99.7% purity), which were purchased from Sigma-Aldrich Ltd. (Singapore). Propylene carbonate (99.7% purity) and anhydrous EC (99% purity) were both obtained from Sigma Aldrich (USA). TiO_2 purity), which nanopowder (21 nm; 99.5% purity), 99.5% purity, iodine (≥ 99.8% purity), and HNO_3 (≥ 99.9% purity) were purchased from Sigma Aldrich in Singapore. Polyethylene glycol (PEG-1000) (Mw 1000; 99% purity) and KI (≥ 99% purity) were obtained from Merck in Germany. Deionized water (Aqua DM) (99.8% purity) was purchased from CV. Chemical Indonesia Multi Sentosa (Indonesia). Tween 80 (with a purity level of ≥99.8%) was purchased from PT Smart Lab in Indonesia. FTO glass (resistivity 10 Ω) was purchased from XinYu Xu Tking Glass Co., China. *Clitoria ternatea L.* was purchased from a local farm (Surabaya, Indonesia).

2.2. Methods

2.2.1. Preparation of the natural dyes

The process of synthesizing organic photosensitizers through extraction is analogous to the method outlined in the research conducted by Kusumawati et al. (2023) [9]. However, a novel stage is carried out with the help of microwave-assisted extraction (MAE) with the objective of reducing the extraction time. In this method, the natural dye obtained from Telang flower (*Clitoria ternatea L.*) is subjected to a series of washes with water until it is thoroughly cleansed. Following this, the natural dye is extracted using the microwave-assisted extraction method with distilled water solvent in a ratio of 1:20 (sample and solvent) for 15 minutes at 280 watts. The MAE conditions (280 W, 15 minutes) were adopted from Hafidl et al. (2026), in which these parameters were established to effectively preserve the structural integrity of the chromophore molecules while significantly reducing extraction time compared to conventional maceration techniques [11]. The extraction solvent was distilled water, rather than acidified organic solvents, to provide an initial matrix with a neutral pH. This enabled precise and unbiased pH adjustments to be made across the entire pH range of 2–12 investigated in this study. This approach ensures that the structural transformations of anthocyanin molecules observed under various pH conditions reflect the effects of pH adjustment alone, without interference from the composition of the extraction solvent. This finding is consistent with the results of previous research by Kusumawati et al. (2023) [9]. The natural dye (anthocyanin) is then subjected to pH conditioning in sequence, namely at pH 2, pH 4, pH 6, pH 8, pH 10, and pH 12. Furthermore, the solvent is evaporated using a Buchi R-300 rotary evaporator.

2.2.2. PEI membrane manufacturing

The production of PEI membranes was performed through the implementation of knife casting technique, in accordance with the procedures established by Kusumawati et al. (2020) and Fachrirakarsie et al. (2024) [4,5] in previous studies.

2.2.3. Preparation of electrolyte

In the formulation process, 0.60 g of Potassium Iodide (KI), 0.09 g of Iodine (I_2), 4.00 g of PC, and 4.00 g of EC were mixed through magnetic stirring at 100 rpm for 1 hour using NESCO LAB MS-H280-Pro. The resulting solution, serving as the electrolyte, was stored in an opaque container with the objective of protecting it from direct sunlight exposure and ensuring optimal stability for subsequent applications.

2.2.4. TiO_2 paste preparation

The TiO_2 paste was prepared according to the procedure established in previous studies [12]. In this process, 0.40 g of TiO_2 was mixed with 0.16 g of PEG 1000. Subsequently, 0.10 mL HNO_3 and 0.80 mL Tween-80 were added to the mixture, which was then stirred for 30 minutes at 100 rpm using a

NESCO LAB MS-H280-Pro magnetic stirrer to ensure even distribution. In the subsequent stage of the procedure, the prepared TiO_2 paste, using the doctor blade method, was applied to an FTO (fluorine-doped tin oxide) anode with an active area of 3.00 cm^2 and a TiO_2 thickness of 0.20 mm. The coated substrate was then subjected to sintering at a temperature of 450°C for 1 hour, with the objective of producing a well-defined product.

The uniformity of the TiO_2 layer on the FTO glass substrate was ensured through the utilization of the doctor blade technique, as has been documented in previous studies [8,12,13]. In this method, TiO_2 paste is applied onto the FTO glass substrate using a blade that is drawn across the surface at a controlled height, thereby producing a thin film of consistent and uniform thickness across the substrate area. This technique has been extensively adopted in the domain of DSSC fabrication for its capacity to facilitate the deposition of reproducible thin-film layers. Following the coating, the electrode was sintered at 450 °C to remove organic binders from the paste and ensure proper adhesion and crystallinity of the TiO_2 film on the substrate. Thereafter, it was cooled before further processing.

2.2.5. Fabrication DSSC

Following the sintering process, the TiO_2 photoanodes were immersed in a 10-mL solution of natural dye for 24 hours, as in a previous study by Estiningtyas et al. (2023) [14]. Subsequently, a precision-cut PEI membrane, made through a combination of casting and electrospinning methods, was 2.0 cm in length and 1.5 cm in width. The membrane was immersed in 1.0 mL of electrolyte for 1 hour. The cathode on an FTO glass substrate received a layer of carbon derived from wax. The configuration of the DSSC circuit was defined as FTO/TiO_2/dye/PEI/Pt/FTO, as depicted in Fig. 1.

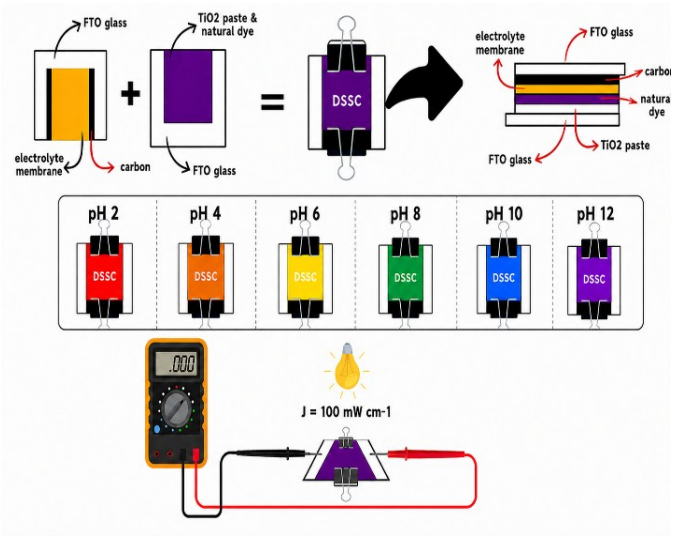

Fig. 1. Fabrication, pH Variation, and Measurement Setup of DSSCs

2.2.6. UV-Vis spectrophotometry

The absorption spectrum of the natural UV photosensitizer was analyzed utilizing Shimadzu UV-1800 UV-Vis Spectrophotometry at 400 - 800 nm.

2.2.7. Fourier transform infrared (FTIR)

The functional groups of natural dyes from various pH conditions were analyzed by means of an FTIR spectrophotometer (Perkin Elmer Spectrum Two). Spectral data was collected in transmission mode at 4000 - 500 cm^{-1}, using scans at 4 cm^{-1} resolution.

2.2.8. Scanning electron microscopy (SEM)

To obtain the surface morphology of the membrane, analysis was carried out using Scanning Electron Microscopy (Zeiss EVO MA-10) at magnifications of 1000x, 3000x, 5000x, and 10,000x.

2.2.9. Differential scanning calorimetry (DSC)

The membrane and TiO_2 thermal stability was evaluated using Linseis STA PT-1000 Differential Scanning Calorimetry (DSC) at room temperature -450 °C (450 K) with a 10.0 °C/min heating rate.

2.2.10. X-Ray diffraction (XRD)

The phase, crystal structure, and degree of crystallinity of the membrane and TiO_2 were analyzed using X-Ray Diffraction (XRD) (PANalytical, X'Pert PRO).

2.2.11. Voltammetry Cyclic

The current and potential changes associated with the color pigments utilized in the DSSC were evaluated through the utilization of a Voltammetry Instrument (797 VA Computrace Metrohm) [7,8]. The HOMO, LUMO, and band gap energy values of natural dyes can be calculated by Eq. 1-3 [12]:

$$E_{HOMO} = -(E_{ox} + 4.40)\ eV \quad (1)$$

$$E_{LUMO} = -(E_{red} + 4.40)\ eV \quad (2)$$

$$E_g = E_{LUMO} - E_{HOMO} \quad (3)$$

2.2.12. Photovoltaic studies

Current and voltage were obtained from measurements using a Krisbow KW08-267 Multimeter at a resistance of 200 kΩ and a voltage of 200 mV to assess the performance of the DSSC circuit. The overall cell performance is determined by FF (Eq. 4) and cell efficiency (η) (Eq. 5), which are performed according to the formula referenced by Kusumawati et al. (2024) [15].

$$FF = \frac{V_{max} \times I_{max}}{V_{oc} \times I_{sc}} \quad (4)$$

$$\eta = \frac{FF \times V_{oc} \times I_{sc}}{P_{in}} \quad (5)$$

2.2.13. Electrochemical impedance spectroscopy (EIS)

The characterization of charge transfer resistance was

conducted through the utilization of electrochemical impedance spectroscopy (EIS) measurements, which were performed over a frequency range of 0.1 Hz to 100 kHz, using the Gamry Reference 3000 instrument, as has been performed in studies conducted by Kusumawati et al. (2023) and Hafidl et al. (2026) [9,11].

3. Results and Discussion

3.1. UV-Vis analysis

Natural dyes in DSSCs play a crucial role in enhancing visible light absorption on TiO_2 substrates, offering advantages such as high availability, simple extraction, high absorption coefficients, cost-effectiveness, non-toxicity, and biodegradability [16,17]. This study evaluates the effect of pH on anthocyanin dyes from butterfly pea flowers (*Clitoria ternatea L.*) extracted using MAE (280 W, 15 min). Spectrophotometric characterization was then conducted over the 400–800 nm range to assess their potential as natural sensitizers for DSSCs.

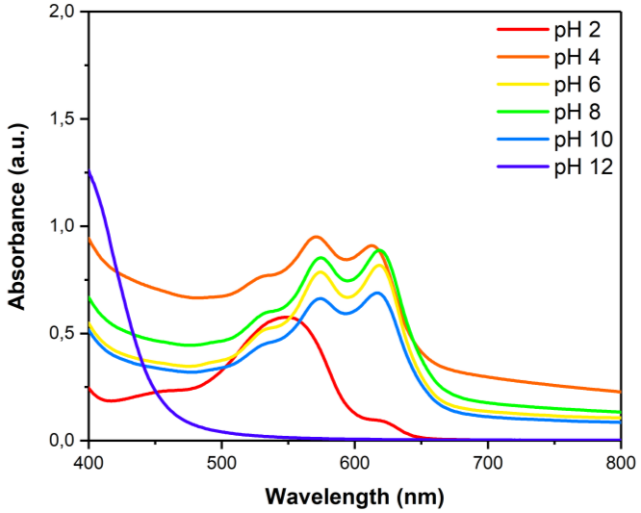

Fig. 2. UV-Vis absorption spectra of anthocyanin extracts at varying pH values

Fig. 2 presents the UV-Vis spectra of anthocyanins at pH values ranging from 2 to 12, exhibiting distinct absorption peaks at 548.92 nm (pH 2); 571.21 and 612.85 nm (pH 4); 574.00 and 618.33 nm (pH 6); 574.46 and 618.78 nm (pH 8); and 574.00 and 616.78 nm (pH 10). No peak was detected at pH 12, likely due to the low anthocyanin concentration, shifting the peak below 460 nm. These results are consistent with those reported by Okello et al. (2022), who reported a shift in the peaks towards 600 nm with decreasing absorbance as pH increased [18].

This pH-dependent absorption behavior differs from concentration-dependent absorption, which follows the Lambert-Beer law [19], as different molecular structures form at each pH. In aqueous solution, anthocyanins exist in five equilibrium forms (Fig. 3): flavylium cation (red), carbinol pseudo-base (colorless), quinoidal base (purple), quinoidal anion (blue), and chalcone (yellowish), with the dominant form determined by the solution pH [16].

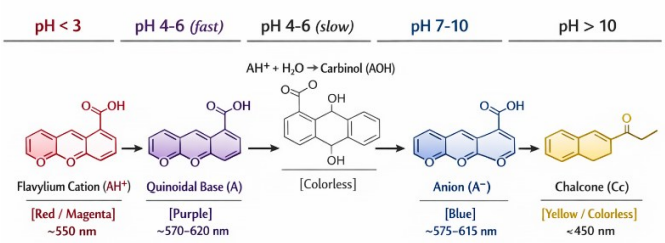

Fig. 3. Schematic illustration of pH-induced structural interconversions of anthocyanins from *Clitoria ternatea L.*, illustrating the equilibrium among five molecular forms: flavylium cation (pH < 3), quinoidal base (pH 4–6), carbinol pseudo-base (pH 4–6), quinoidal anion (pH 7–10), and chalcone (pH > 10)

The bathochromic shift from 550 nm (pH 2) to 575–620 nm (pH 8) is indicative of structural equilibrium transitions: flavylium cation (pH <3) → quinoidal base (pH 4–6) → quinoidal anion (pH 7–10) → chalcone (pH >10) [20]. At pH <3, the flavylium cation (AH^+) dominates with a modest absorption at 550 nm and minimal light absorption capacity. Increasing the pH value to a range of 4–6 has been shown to trigger two simultaneous reactions. Firstly, deprotonation forms the neutral quinoidal base (A) with two peaks at 570–620 nm, which is the most intense. Secondly, nucleophilic hydration forms the colorless carbinol pseudo-base (AOH). At pH 7–10, further deprotonation yields the blue quinoidal anion (A^-) with progressively decreasing absorption, while the AOH tautomerizes into chalcone (Cc) absorbing below 450 nm. At pH >10, the equilibrium shifts entirely towards the chalcone and carbinol forms, resulting in negligible visible light absorption at pH 12 [21,22].

FTIR analysis (Fig. 4) confirms that these transformations do not alter the functional groups; hydroxyl, carbonyl, and aromatic C=C remain intact but only modify the degree of π-electron conjugation, which is sensitively detected by UV-Vis spectroscopy. This explains why pH 4 is the optimal condition for DSSCs: the quinoidal base formed maximizes the conjugated chromophore system, thereby enhancing absorption efficiency at 500–650 nm, followed by pH 6 and 8, which exhibit similar characteristics with slightly lower intensity. The dual-peak pattern at intermediate pH values has the potential to improve photon capture across multiple wavelengths, ultimately enhancing the photovoltaic performance of DSSCs.

3.2. FTIR analysis

In this study, Fourier Transform Infrared (FTIR) Fourier Transform Infrared (FTIR) analysis of anthocyanin extract from butterfly pea flowers (*Clitoria ternatea L.*) was conducted over a wavenumber range of 4000–500 cm^{-1} across pH variations of 2–12. The consistent spectral profiles observed across all pH conditions indicate the structural stability of anthocyanin molecules, which is a critical characteristic for DSSC applications.

The FTIR spectrum in Fig. 4 reveals a series of characteristic absorption bands that comprehensively reflect the molecular structure of anthocyanins. The band at 803.17 cm^{-1} indicates out-of-plane C–H aromatic bending vibrations of substituted rings, supported by broad absorption in the 600–900 cm^{-1} range. The peaks at 1044.88 and 1087.28 cm^{-1} correspond to C-O, either stretching and C-H alkene bending vibrations, while the band at 1416.91 cm^{-1} confirms the presence of aromatic

C=C stretching as a fundamental structural component of anthocyanins [20]. Furthermore, the absorption at 1651.60 cm^{-1} indicates alkene C=C stretching, asymmetric C–H stretching at 2974.49 cm^{-1} is characteristic of alkane groups, and O–H stretching at 3338.08 cm^{-1} suggests the presence of alcohol or carboxylic acid functional groups. The minimal absorption in the 1300–1000 cm^{-1} region is indicative of the absence or low concentration of O–R functional groups [23].

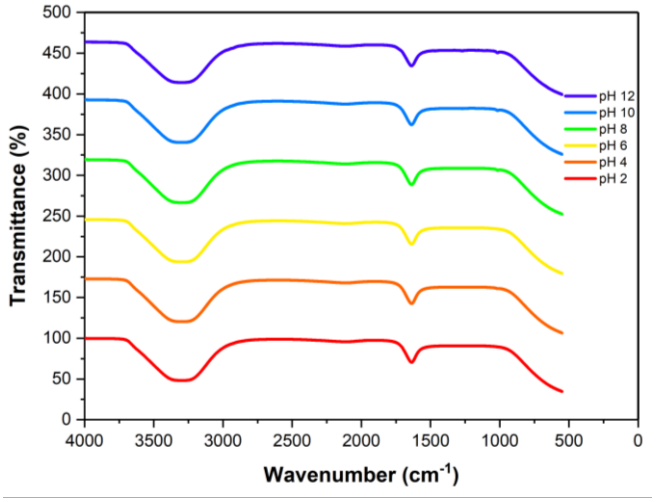

Fig. 4. FTIR spectra of anthocyanin extracts at varying pH values

The absorption at 1710 cm^{-1}, indicative of C=O stretching from carbonyl groups, plays a significant role in the light absorption capability of anthocyanins in the visible spectrum, thereby directly contributing to improved DSSC efficiency. This hypothesis is further substantiated by the observation of reduced current density under visible light in comparison to UV illumination, thereby confirming the dominant response of TiO_2 in the UV region and thus indicating electron excitation processes [24].

A comparison of FTIR spectra across all pH variations revealed no new peaks or significant shifts in absorption bands. This finding indicates that pH changes do not induce new chemical bond formation and that the observed structural alterations are reversible rather than indicating permanent degradation. The core functional groups of anthocyanins, including hydroxyl, carbonyl, aromatic C=C, and ether groups, remained structurally intact across all pH conditions. These findings are consistent with UV-Vis data showing that shifts in absorption maxima reflect only changes in protonation states and chromophore conjugation. Collectively, the FTIR and UV-Vis data complement each other in confirming the molecular structural integrity of anthocyanins and the dynamic interconversion among flavylium cation, quinoidal base, and chalcone forms. This collectively confirms the potential of butterfly pea anthocyanins as stable natural sensitizers for DSSC applications across varying pH conditions.

3.3. SEM analysis

The surface morphology of the PEI membrane was analyzed by means of SEM at magnifications in the range of 1,000x to 10,000x (Fig. 5). The micrographs reveal a porous structure with uniformly distributed hierarchical features. At low magnifications, Fig. 5(a) and 5(b) reveal a uniform surface topography with an interconnected polymer network. In contrast, at higher magnifications, Fig. 5(c) and 5(d) demonstrate a three-dimensional microstructure with varied micropores becomes apparent. The membrane surface appears to be smooth, homogeneous, dense, and porous. As posited by Kusumawati et al. (2019), this morphology facilitates enhanced conductivity by minimizing electrical resistance at maximum voltage and current, while concurrently reducing ion accumulation induced by heat or light reflection [3]. Fachrirakarsie et al. (2024) further reported that this morphology enhances the quality of contact between the membrane and the electrode [5].

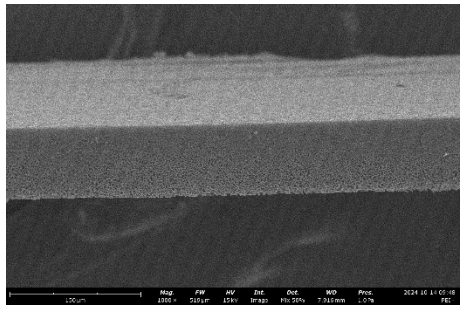

(a)

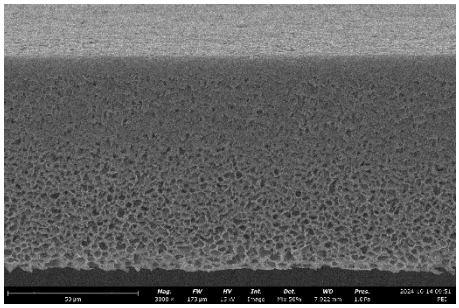

(b)

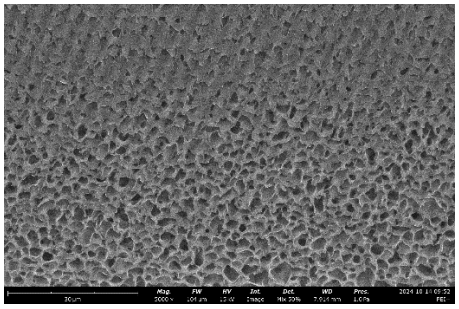

(c)

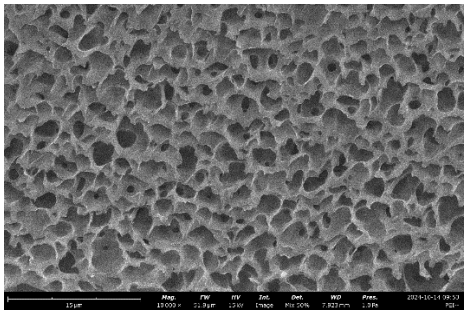

(d)

Fig. 5. SEM analysis of membran PEI with magnification: (a) 1.000x, (b) 3.000x, (c) 5.000x, (d) 10.000x

The porous architecture has been shown advantageous for DSSC applications, as it is able to provide a large internal surface area that supports electrolyte retention, ion transport, and efficient redox couple mobility and dye regeneration. The cross-sectional morphology reveals an asymmetric structure with sponge- and finger-like pores [3,4], consistent with the findings of Fachrirakarsie et al. (2024) [5]. This asymmetric structure is characteristic of membranes fabricated via non-solvent-induced phase separation (NIPS), wherein the top layer undergoes solidification prior to the formation of an expanded structure by the bottom layer [25]. The membrane thickness of approximately 700µm, with a dense skin layer thinner than the underlying porous sublayer, further confirms this asymmetric characteristic.

The PEI membrane fabricated by Kusumawati et al. (2020) [4] demonstrated a porosity of 19.77% and a pore size of 0.515 nm. Conversely, the pure PEI membrane reported by Kusumawati et al. (2019) [3] demonstrated a porosity of 22.17% with a pore size of 0.745 nm. These parameters are consistent with the hierarchical architecture as observed in Fig. 5(c) and 5(d), where micropores support electrolyte retention and finger-like macropores facilitate ion transport. The homogeneously distributed interconnected polymer network further facilitates multidirectional ion transport while ensuring mechanical stability during cell assembly and operation.

The morphological characteristics of the PEI membrane are consistent with the extant literature associating similar pore architectures with enhanced DSSC performance. As reported by Zhu et al. (2022), there was an improvement in ionic conductivity in porous polymer membranes [26]. In addition, Wang et al. (2021) correlated similar interconnected morphologies with better electrolyte retention and DSSC stability [27]. Furthermore, the hierarchical pore structure observed in Fig. 5(c) and 5(d) has been associated with enhanced electron transport and reduced recombination rates. Collectively, the PEI membrane possesses an optimal pore architecture, adequate porosity, nanoscale pore size, and asymmetric structure that comprehensively supports high DSSC performance. Further electrochemical and photovoltaic characterization is required to correlate this morphology with specific DSSC performance parameters.

3.4. Differential scanning calorimetry (DSC) analysis

The DSC analysis depicted in Fig. 6 provides a comprehensive overview of the thermal stability of the main DSSC components. The DSC curve of the PEI membrane presented in Fig. 6(a) demonstrates good thermal stability up to 100°C with no significant thermal transitions and a glass transition temperature (Tg) of approximately 215°C, thus offering a wide safety margin for long-term flexible DSSC operation [5]. This stability directly ensures that the barrier properties and optical transparency of PEI remain consistent during operation, which is a critical factor in maintaining overall performance of the device.

In line with this, the DSC curve of TiO_2 as depicted in Fig. 6(b) further confirms adequate thermal stability, as evidenced by the absence of substantial phase transitions or degradation up to 100°C. This finding confirms that the anatase phase of TiO_2 remains stable within the DSSC operating temperature range, thereby preserving its photocatalytic properties and electronic conductivity. Furthermore, the exothermic peak observed in the range of 600–700°C indicates an anatase-to-rutile phase transformation, which occurs well above the normal DSSC operating temperature. The high enthalpy value associated with this peak reflects good TiO_2 crystallinity, which plays a significant role in predicting and maintaining optimal device performance in DSSC applications.

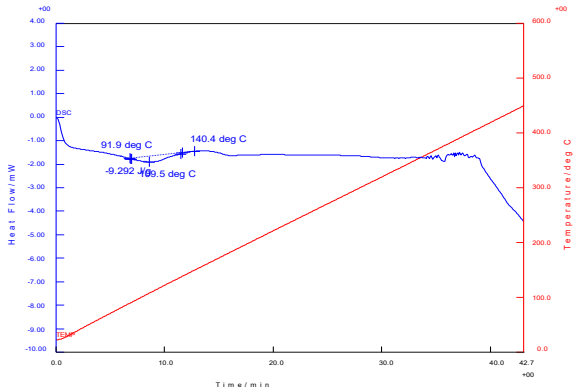

(a)

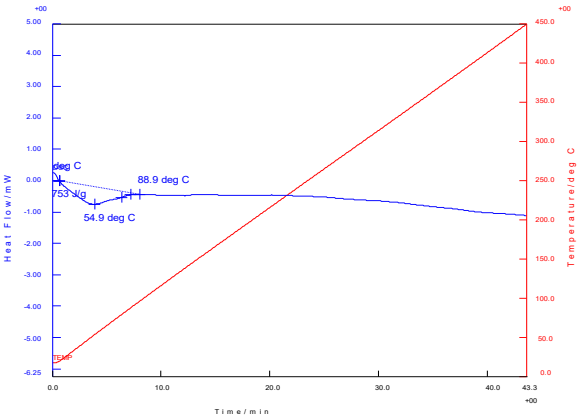

(b)

Fig. 6. DSC curve of (a) PEI membrane; (b) TiO_2

3.5. X-Ray diffraction (XRD) analysis

The crystal structure of DSSC materials was analyzed through X-ray diffraction (XRD), with the results presented in Fig. 7(a) through 7(g). As illustrated in Fig. 7(a), the PEI membrane exhibits amorphous characteristics, as evidenced by the broad diffraction pattern observed without any sharp crystalline peaks. This amorphous nature of the material provides good mechanical flexibility, optical transparency, and adequate thermal stability, thereby rendering PEI a suitable substrate for DSSC fabrication and operation.

In contrast to the PEI sample, the XRD curve of TiO_2 in Fig. 7(b) exhibits sharp, high-intensity diffraction peaks, indicating good crystallinity with a mixed anatase and rutile phase. This high crystallinity has been demonstrated to play a significant role in enhancing electron mobility and reducing electron trapping, thereby enabling more efficient electron transfer from the dye to the TiO_2 conduction band. To enhance comprehension of the contributions made by each phase, analyses of crystallinity and crystallite size were performed separately.

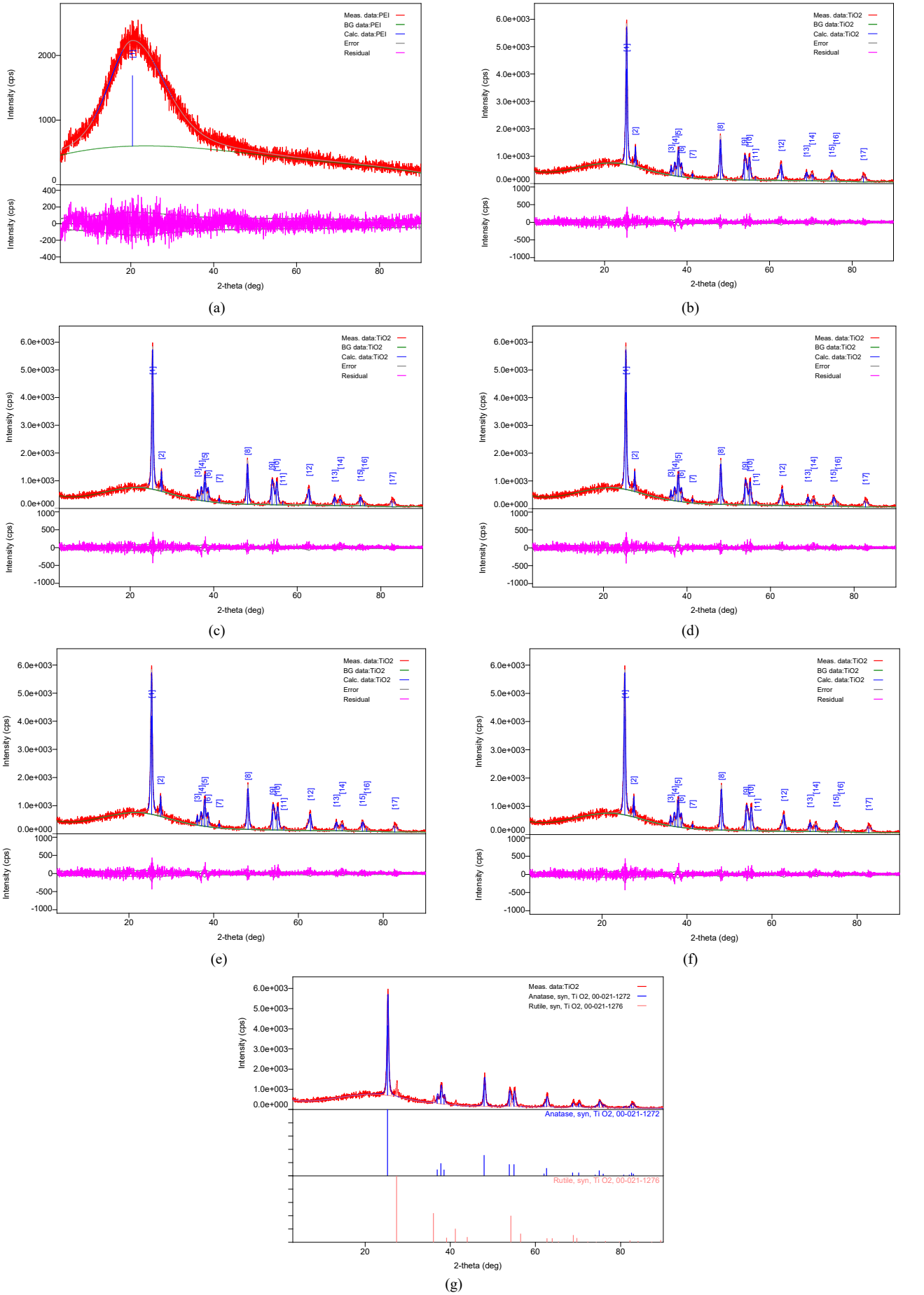

Fig. 7. XRD curves of (a) PEI membrane; (b) TiO_2; (c) crystallinity of anatase TiO_2; (d) crystallite size of anatase TiO_2; (e) crystallinity of rutile TiO_2; (f) crystallite size of rutile TiO_2; (g) phase identification of TiO_2

As illustrated in Fig. 7(c) and 7(d), the anatase phase exhibits high crystallinity with a regulated nanocrystal size calculated in accordance with the Scherrer equation. The small crystallite size yields a high specific surface area, thereby optimizing dye adsorption, while the low strain value serves to minimize crystal defects and recombination centers. It is evident that these conditions directly contribute to enhanced Jsc and FF in DSSC performance. Conversely, Fig. 7(e) and 7(f) demonstrate that the rutile phase has a larger crystallite size in comparison to anatase. Whilst the photocatalytic activity is lower, the larger crystal size enhances light scattering at longer wavelengths. This is further supported by the higher refractive index ($n \approx 2.7$) of rutile in comparison to anatase ($n \approx 2.5$), thereby increasing the optical path length and overall light absorption within the DSSC.

A comprehensive overview of the TiO_2 phase composition is demonstrated in Fig. 7(g), which identifies the anatase peak at $2\theta \approx 25.3°$ and the rutile peak at $2\theta \approx 27.4°$. This indicates an optimal phase ratio for DSSC applications: dominant anatase (70–85%) for electron injection and transport, and minor rutile (15–30%) for light scattering. The absence of impurity phases such as brookite or TiO_2-B confirms the overall purity of the material. The combination of both phases forms an anatase-rutile heterojunction capable of suppressing recombination rates through favorable energy band alignment, ultimately enhancing the overall efficiency of the DSSC application.

3.6. Voltammetry cyclic analysis

To enhance the overall efficiency of DSSCs and optimize the effectiveness of natural dyes as photosensitizers, it is imperative that the band gap energy of the dye is reduced relative to that of the TiO_2 semiconductor. It has been demonstrated that the effectiveness of the extracted dye increases in proportion to the decrease in the difference between the highest occupied molecular orbital (HOMO) and the lowest unoccupied molecular orbital (LUMO) values. The dye's capacity for regeneration is indicative of the ease with which electrons can be transferred from the electrolyte I^- or I_3^- to the HOMO band of the material [28]. This phenomenon is related to the fact that dye electrons can be stimulated more easily from the valence band to the conduction band when their energy is sufficiently minimal. TiO_2 has been demonstrated to influence the conduction band, thereby aligning its impact with the energy level of the LUMO dye molecules and facilitating electron injection. Specifically, the anatase phase exhibits a band gap energy of 3.2 eV, while the rutile phase demonstrates a slightly lower value of 3.0 eV. The determination of the band gap energy of the dye refers to equations 1-3.

Table 1. The HOMO, LUMO, and band gap values for anthocyanin extracts at varying pH values

Dye (various pH)	HOMO (eV)	LUMO (eV)	Eg (eV)
pH 2	-3.3203	-2.9481	0.3722
pH 4	-4.1597	-4.0281	0.1316
pH 6	-3.5822	-3.3068	0.2754
pH 8	-4.1595	-4.0072	0.1523
pH 10	-3.3136	-2.9147	0.3989
pH 12	-3.3257	-2.8531	0.4726

It is evident from the energy band gap values obtained for each dye at varying pH levels that anthocyanins from telang flowers (*Clitoria ternatea L.*) can be utilized as sensitizers in DSSCs as they satisfy the requirements of DSSC dyes. The LUMO value of each dye is significantly higher than the TiO_2 conduction value of -4.0 eV, which is important to ensure the electron injection capability of the excited dye into the semiconductor.

As demonstrated in Table 1, each pH variation exhibits an energy gap between 0.1316 and 0.4726 eV. pH 4 emerges as the most favorable condition with the smallest band gap value of 0.1316 eV. This finding indicates the suitability and stability of the dye extract for DSSC applications. This reduction in band gap size has been shown to facilitate more efficient electron transfer, a process which is of importance to the long-term performance of DSSCs. A reduced band gap thus indicates a narrower energy difference between the valence and conduction bands, thereby facilitating electron movement and enhancing electrical conductivity. The lower HOMO-LUMO energy gap promotes a shift towards longer wavelengths in the absorption spectrum, known as a bathochromic shift, which is favorable for enhancing the efficiency of photovoltaic devices. The pH 4 condition demonstrates the most optimal characteristics for DSSC applications, exhibiting the smallest energy band gap, thus facilitating more effective electron transfer.

3.7. Photovoltaic studies

The assessment of the DSSC circuit was conducted to measure the open voltage (Voc), short circuit current (Jsc), fill factor (FF), and efficiency (η) using a multimeter under lamp illumination with an intensity of 100 mW/cm². The overall cell performance is determined by FF and cell efficiency (η) calculated using equation (4-5). In this equation, Vmax denotes the maximum output voltage, Imax signifies the maximum output current, Isc indicates the short circuit current, Voc indicates the open circuit voltage, and Pin represents the input power [8].

Table 2. Photovoltaic parameters of DSSC

Dye (various pH)	Voc (mV)	Isc (mA/cm²)	FF (%)	Efficiency (%)
pH 2	242	0.0092	17.92	0.74
pH 4	597	0.0119	5.60	2.37
pH 6	344	0.0109	10.63	1.25
pH 8	568	0.0114	6.13	2.17
pH 10	258	0.0095	16.29	0.81
pH 12	167	0.0085	28.10	0.47

This present study examines the current-voltage (I-V) characteristics of DSSCs utilizing anthocyanin dye from telang flowers (*Clitoria ternatea L.*) under diverse pH conditions. The performance of DSSCs is evaluated through Voc, Isc, and FF parameters. The impact of utilizing anthocyanin as a natural photosensitizer on the performance of DSSC is evident in the I-V curves (Fig. 8) and photovoltaic characterization presented in Table 2.

The effectiveness of extract from telang flowers, indicates a promising potential as a photosensitizer in DSSCs. It has been demonstrated that anthocyanin pigments possess the capacity to capture light at wavelengths suitable for DSSC mechanisms, thereby facilitating the conversion of photons into electricity. It is evident that variations in pH provide divergent absorption ranges of sunlight, potentially enhancing the efficiency of DSSCs. As a photosensitizer, anthocyanin pigments exhibit adequate chemical and photochemical stability.

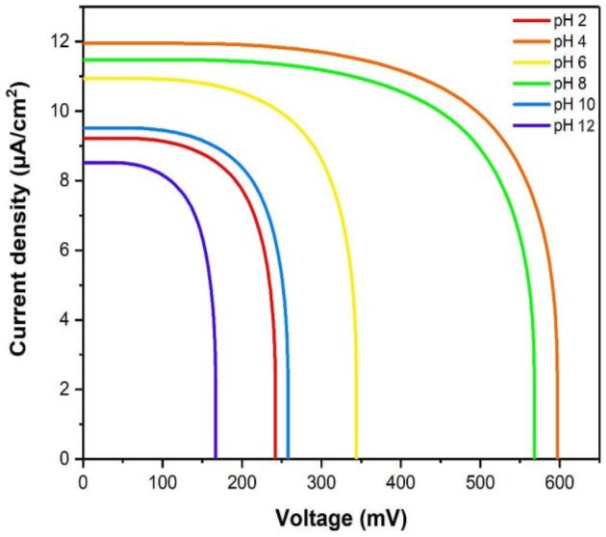

Fig. 8. The I-V curves were obtained for DSSC sensitized with anthocyanin extracts at varying pH values

Of the six pH variations tested, the order of efficiency observed was pH 4 (2.37%) > pH 8 (2.17%) > pH 6 (1.25%) > pH 10 (0.81%) > pH 2 (0.74%) > pH 12 (0.47%). The most effective various pH was found at pH 4, which yielded Isc, Voc, FF, and photoconversion efficiency (η) values of 0.0119 mA/cm^2, 597 mV, 5.60%, and 2.37%, respectively. This finding indicates that the dye extract at pH 4 retains its stability and efficacy under DSSC operational conditions. It is evident from the alignment with previous band gap analysis that the dye at pH 4 exhibits a reduced band gap. A reduced band gap value signifies faster electron transfer due to an increase in the number of conjugated chains. The band gap data demonstrated that the pH 4 dye exhibited the smallest band gap among the other pH variations, consequently resulting in enhanced performance due to increased solar light absorption and more efficient utilization of photon energy [29]. Furthermore, the enhancement of DSSC efficiency is determined by the optimal TiO_2 thickness of 0.2 mm and the optimal PVDF NF polymer electrolyte membrane, as reported by Kusumawati et al. (2024) [15].

The I-V curves demonstrate that pH 4 provides the optimal performance with high open circuit voltage and optimal current density. The pH 4 exhibits the most ideal curve characteristics exhibiting a combination of high Voc and adequate Jsc, thereby resulting in the highest efficiency. The molecular structure of anthocyanin at pH 4 in the form of a quinoidal base allows for optimal light absorption and efficient electron transfer to TiO_2. This assertion is indicated by reasonable fill factor values, although these are not as elevated as those recorded at other pH extremes.

3.8. Electrochemical Impedance Spectroscopy (EIS)

Nyquist plots from the EIS analysis presented in Fig. 9 illustrate the electrochemical impedance characteristics of anthocyanin dye from *Clitoria ternatea L*. at varying pH levels (2–12). Each condition produces a different semicircular diameter that directly correlates with the charge transfer resistance (Rct) at the photoanode/electrolyte interface. pH 12 exhibits the largest semi-circular diameter, with a Z_{Re} value approaching 1750 Ω, suggesting remarkably high resistance and suboptimal performance. In contrast, pH 4 exhibits the smallest semi-circular diameter with Z_{Re} of only around 100–150 Ω, followed by pH 8 (350 Ω), pH 6 (700 Ω), pH 10 (1050 Ω), and pH 2 (1300 Ω). These results reflect significant differences in charge-transfer efficiency across pH conditions.

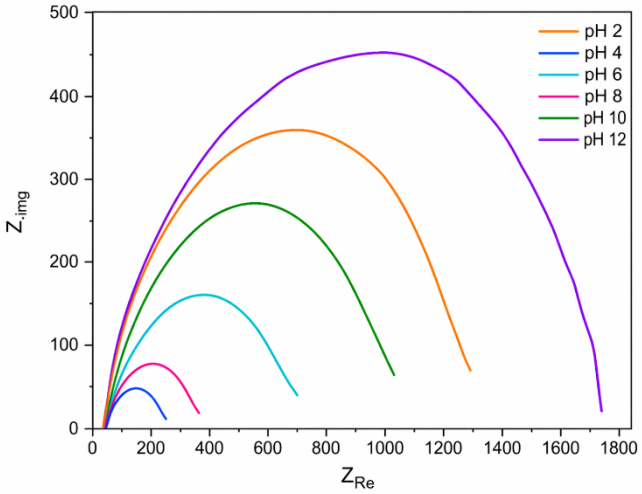

Fig. 9. Nyquist Plot Obtained from the EIS Spectrum of DSSC with Anthocyanin Extracted at Various pH

A more detailed analysis reveals that Rct reaches its lowest value at pH 4, indicating the most efficient interfacial charge transport between the anthocyanin dye and the TiO_2/electrolyte system. This finding is consistent with the dominance of the quinoidal base structure at that pH, which maintains optimal π-conjugation and maximum UV-Vis absorption. Conversely, extreme conditions at pH 2 and pH 12 show the highest Rct values with hindered electron mobility and increased recombination rates, owing to the transformation of anthocyanin into flavylium cation and chalcone forms, respectively, which disrupt the molecular conjugation system.

The optimal performance at pH 4 can be attributed to the superior sensitizing ability of anthocyanin, high TiO_2 surface coverage, and optimal redox potential adjustment under mildly acidic conditions. The report of Masud and Kim (2023) indicated that optimal pH conditions facilitate stable interactions between dyes and TiO_2 substrates [30]. Conversely, elevated alkalinity (pH 12) degrades anthocyanin into the chalcone form that loses visible light absorption, while excessive acidity (pH 2) stabilizes the flavylium cation that is less effective in electron injection, as confirmed by Vij et al. (2023), who found that pH-induced disruption of the dye's electronic structure directly leads to reduced DSSC performance [31]. Consequently, an optimal balance between molecular stability, adsorption behavior, and charge kinetics is

achieved at a pH of 4, as reflected in a combination of minimal charge transfer resistance and maximal photovoltaic efficiency. The low Rct value corresponds to fast electron exchange and fewer recombination losses at the TiO_2/dye/electrolyte interface.

4. Conclusion

This study successfully demonstrates that pH optimization is a critical parameter for enhancing the photovoltaic performance of dye-sensitized solar cells (DSSCs) utilizing anthocyanin extracts from *Clitoria ternatea L*. as natural photosensitizers coupled with polyetherimide (PEI) polymer membrane electrolytes. A comprehensive characterization revealed that pH 4 represents the optimal condition, exhibiting maximum dual absorption peaks at 571.21 nm and 612.85 nm. These correspond to the magenta-colored quinoidal base structure, which possesses superior light-harvesting capabilities, the narrowest energy bandgap (0.1316 eV) with HOMO at -4.1597 eV and LUMO at -4.0281 eV, which are optimally aligned with the TiO_2 conduction band (-4.0 eV), and the highest DSSC efficiency of 2.37% with Voc = 597 mV, Jsc = 0.0119 mA/cm^2, FF = 5.60%, and minimum charge transfer resistance Rct = 100–150 Ω. The PEI membrane exhibited asymmetric morphology with a hierarchical porous structure, 12.77% crystallinity, and excellent thermal stability up to 500 °C, thereby providing optimal electrolyte retention and ion transport. FTIR analysis confirmed excellent structural stability across all pH conditions (pH 2-12) without the formation of new chemical bonds, thus demonstrating chemical compatibility, which is essential for DSSC applications. The strong correlation between UV-Vis absorption characteristics, energy bandgap values, charge transfer resistance, and photovoltaic efficiency validates that the formation of a quinoidal base structure at pH 4 through partial deprotonation of hydroxyl groups enhances molecular conjugation, maximizes visible light absorption, minimizes charge transfer resistance, and accelerates electron transfer processes. The findings of this study establish pH 4 optimization as a critical strategy for enhancing DSSC efficiency in environmentally sustainable photovoltaic systems. This confirms the potential of optimizing natural dye extraction conditions as an effective approach to advance cost-effective, reproducible, and environmentally friendly solar cell technology for practical renewable energy applications.

Acknowledgements

The author acknowledges the financial support provided by the Indonesian Ministry of Education, Culture, Research, and Technology through national competitive research grants.

References

1. Q. Hassan, P. Viktor, T. J. Al-Musawi, B. M. Ali, S. A. H. M. Alzoubi, A. K. Al-Jiboory, A. Z. Sameen, H. M. Salman, and M. Jaszczur, *The renewable energy role in the global energy transformations*, Renew. Energy Focus. 48 (2024) 100545.
2. S. Kaliramna, S. S. Dhayal, R. Chaudhary, S. Khaturia, K. L. Ameta, and N. Kumar, *A review and comparative analysis of different types of dyes for applications in dye-sensitized solar cells*, Braz. J. Phys. 52 (2022) 136.
3. N. Kusumawati, P. Setiarso, A. B. Santoso, S. C. Wibawa, and S. Muslim, *The development of PVDF/PEI blended membrane: effect of stirring time on membrane characteristics and performance*, Rasayan J. Chem. 12(2) (2019) 975-986.
4. N. Kusumawati, A. B. Santoso, S. C. Wibawa, P. Setiarso, and S. Muslim, *Development of a new polymer membrane: polyvinylidene fluoride/polyetherimide blend membrane*, Int. J. Adv. Sci. Eng. Inf. Technol. 10(6) (2020).
5. F. F. Fachrirakarsie, and N. Kusumawati, *The effect of polyetherimide polymer membrane composition on the performance efficiency of dye sensitized solar cell (DSSC) based on natural photosensitizer of butterfly pea flowers*, J. Pijar MIPA. 19(3) (2024) 507–513.
6. E. O. Alegbe, and T. O. Uthman, *A review of history, properties, classification, applications and challenges of natural and synthetic dyes*, Heliyon. 10 (2024) e33646.
7. N. Kusumawati, P. Setiarso, S. Muslim, N. Zakiyah, K. Rahmawati, and F. F. Fachrirakarsie, *Optimizing dye-sensitized solar cell (DSSC) performance through synergistic natural dye combinations from Beta vulgaris L., Curcuma longa L., and Pandanus amaryllifolius*, Indones. J. Chem. 24(6) (2024) 1675-1687.
8. K. Rahmawati, N. Kusumawati, P. Setiarso, S. Muslim, N. Zakiyah, and F. F. Fachrirakarsie, *Optimizing dye-sensitized solar cell efficiency with a triple blend of Caesalpinia sappan L., Dracaena angustifolia, and Clitoria ternatea L.*, Molekul. 20(1) (2025) 73 – 85.
9. N. Kusumawati, P. Setiarso, A. B. Santoso, S. Muslim, Q. A'yun, and M. M. Putri, *Characterization of poly(vinylidene fluoride) nanofiber-based electrolyte and its application to dye-sensitized solar cell with natural dyes*, Indones. J. Chem. 23(1) (2023) 113-126.
10. T. S. Kumar, S. Shalini, T. A. Roy, S. Prasanna, R. Balasundaraprabhu, and S. Sundaram, *Solvent selection for anthrocyanin dye extraction from Kigelia Africana and Hibiscus sabdariffa for dye sensitized solar cells*, J. Photochem. Photobiol. 20 (2024) 100233.
11. A. N. Al Hafidl, N. Kusumawati, P. Setiarso, S. Samik, M. M. S. Basukiwardojo, and K. Rahmawati, *Effect of pH on brazilin extraction from sappanwood (Caesalpinia sappan L.) and its impact on the efficiency of natural dye-sensitized solar cells (DSSCs)*, Sci. Technol. Indones. 11(2) (2026) 378–388.
12. P. Setiarso, R. V. Harsono, and N. Kusumawati, *Fabrication of dye sensitized solar cell (DSSC) using combination of dyes extracted from curcuma (Curcuma xanthorrhiza) rhizome and binahong (Anredera cordifolia) leaf with treatment in pH of the extraction*, Indones. J. Chem. 23(4) (2023) 924-936.
13. F. F. Fachrirakarsie, N. Kusumawati, N. Zakiyah, R. N. Safitri, S. Muslim, and K. Rahmawati, *Effect of dye combination and acidity on efficiency of dye sensitized solar cells*, ASEAN J. Chem. Eng. 26(1) (2026) 1-15.
14. I. W. Estiningtyas, N. Kusumawati, P. Setiarso, S. Muslim, N. T. Rahayu, R. N. Safitri, N. Zakiyah, and F. F. Fachrirakarsie, *Effect of natural dye combination and pH extraction on the performance of dye-sensitized photovoltaics solar cell*, Int. J. Renew. Energy Dev. 12(6) (2023) 1054-1060.
15. N. Kusumawati, P. Setiarso, S. Muslim, Q. A. Hafidha, S. A. Cahyani, and F. F. Fachrirakarsie, *Optimization thickness of photoanode layer and membrane as electrolyte trapping medium for improvement dye-sensitized solar cell performance*, Sci. Technol. Indones. 9(1) (2024) 7-16.

16. N. Y. Amogne, D. W. Ayele, and Y. A. Tsigie, *Recent advances in anthocyanin dyes extracted from plants for dye sensitized solar cell,* Mater. Renew. Sustain. Energy. 9 (2020) 23.
17. A. Debnath, S. K. Bhattacharjee, R. Sutradhar, C. Debnath, S. A. Hussain, D. Bhattacharjee, *A review on natural dyes as a sensitizer in dye-sensitized solar cell*, Interactions. 245 (2024) 325.
18. A. Okello, B. O. Owuor, J. Namukobe, D. Okello, and J. Mwabora, *Influence of the pH of anthocyanins on the efficiency of dye sensitized solar cells*, Heliyon. 8 (2022) e09921.
19. A. Okello, B. O. Owuor, J. Namukobe, D. Okello, and J. Mwabora, *Influence of concentration of anthocyanins on electron transport in dye sensitized solar cells*, Heliyon. 7 (2021) e06571.
20. P. Prakash, B. Janarthanan, M. Ubaidullah, A. M. Al-Enizi, S. N. B. Alanazi, R. I. Alkhalifah, and M. Ilyas, *Optimization, fabrication, and characterization of anthocyanin and carotenoid derivatives based dye-sensitized solar cells*, . King Saud Univ. Sci. 35 (2023) 102625.
21. H. Xue, J. Zhao, Y. Wang, Z. Shi, K. Xie, X. Liao, and J. Tan, *Factors affecting the stability of anthocyanins and strategies for improving their stability: A review*, Food Chem. X. 24 (2024) 101883.
22. N. Basilio, A. J. Parola, D. Sousa, V. Petrow, L. Cruz, V. Freitas, and F. Pina, *Achieving Complexity at the Bottom: Molecular Metamorphosis Generated by Anthocyanins and Related Compounds*, ACS Omega. 6 (2021) 30172-30188.
23. T. Rajaramanan, F. H. Gourji, Y. Elilan, S. Yohi, M. Senthilnanthanan, P. Ravirajan, and D. Velauthapillai, *Natural sensitizer extracted from Mussaenda erythrophylla for dye-sensitized solar cell*, Sci. Rep. 13 (2023) 13844.
24. E. P. Mukhokosi, T. Mohammed, N. Loyce, N. L. Botha, M. Maaza, and D. Velauthapillai, *Co-sensitization effect of chlorophyll and anthocyanin on optical absorption properties and power conversion efficiency of dye-sensitized solar cells,* J. Korean Phys. Soc. 84 (2024) 858-869.
25. S. L. Duraikkannu, R. Castro-Munoz, and A. Figoli, *A review on phase-inversion technique-based polymer microsphere fabrication*, Colloid Interface Sci. Commun. 40 (2021) 100329.
26. Y. Zhu, W. Wu, M. Gao, J. Yan, and B. Wang, *Molecular compatibility and hydrogen bonding mechanism of PES/PEI blends*, Polymers. 14 (2022) 3046.
27. Y. Wang, and S. Sun, *Multiscale pore structure characterization based on SEM images*, Fuel. 289 (2021) 119915.
28. J. J. Makangara, M. G. Sahini, and N. S. Babu, *Theoretical and conceptual framework to design D-π-A type organic dyes for application dye-sensitized solar cells*, J. Indian Chem. Soc. 101 (2024) 101118.
29. P. Zhou, B. Lin, R. Chen, Z. An, X. Chen, Q. An, and P. Chen, *Effect of extending the conjugation of dye molecules on the efficiency and stability of dye-sensitized solar cells*, ACS Omega. 6 (2021) 30069-30077.
30. M. Masud, and H. K. Kim, *Redox shuttle-based electrolytes for dye-sensitized solar cells: comprehensive guidance, recent progress, and future perspective,* ACS Omega. 8(7) (2023) 6139–6163.
31. T. Vij, P. P. Anil, R. Shams, K. K. Dash, R. Kalsi, V. K. Pandey, E. Harsanyi, B. Kovacs, and A. M. Shaikh, *A comprehensive review on bioactive compounds found in Caesalpinia sappan*, Molecules. 28(17) (2023) 6247.